

# Buddy Compression: Enabling Larger Memory for Deep Learning and HPC Workloads on GPUs

Esha Choukse  
*University of Texas At Austin*  
*esha.choukse@utexas.edu*

Mattan Erez  
*University of Texas at Austin*  
*mattan.erez@utexas.edu*

Michael Sullivan  
*NVIDIA*  
*misullivan@nvidia.com*

Jeff Pool  
*NVIDIA*  
*jpool@nvidia.com*

Mike O'Connor  
*NVIDIA/University of Texas at Austin*  
*moconnor@nvidia.com*

David Nellans  
*NVIDIA*  
*dnellans@nvidia.com*

Steve Keckler  
*NVIDIA*  
*skeckler@nvidia.com*

## ABSTRACT

GPUs offer orders-of-magnitude higher memory bandwidth than traditional CPU-only systems. However, GPU device memory tends to be relatively small and the memory capacity can not be increased by the user. This work proposes Buddy Compression, a scheme to increase both the effective GPU memory capacity and bandwidth, while avoiding the downsides of conventional memory-expansion techniques. Buddy Compression compresses GPU memory, splitting each compressed memory entry between high-speed device memory and a slower-but-larger disaggregated memory pool or system memory. Highly-compressible memory entries will be accessed completely from device memory, while incompressible entries source their data concurrently utilizing both, on-GPU, and off-GPU memory requests. Increasing the effective GPU memory capacity enables users to run larger memory footprint HPC workloads and larger batch-sizes or models for deep learning training. We show that Buddy Compression achieves an average compression ratio of 1.9x for representative HPC applications and 1.5x for deep learning workloads, with a performance within 2% of an ideal system containing 100% high speed and high capacity memory, making it an ideal candidate for developers who can utilize modest amounts of additional memory capacity with minimal performance penalty.

## 1. INTRODUCTION

GPUs are widely used for many high-memory-footprint applications, including those for High Performance Computing (HPC) and Deep Learning (DL). HPC applications like weather prediction and the modeling of fluid and molecular dynamics have grown to require very large models [1, 2]. DL, one of the most important use-cases for GPUs today, is also developing in a direction where either the model sizes are too big to run on GPUs, or they are large enough such that the only a small batch size can fit on the GPU, resulting in low utilization, and accuracy issues [3, 4].

Today, applications with large memory footprints must either (i) scale out to many GPUs for capacity purposes (in-efficient resource utilization) [5, 6], (ii) explicitly orchestrate

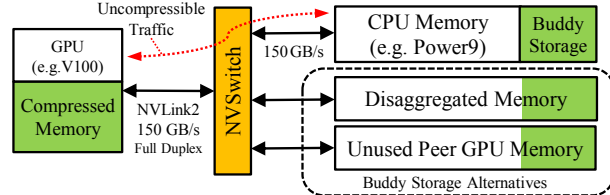


Fig. 1: A view of the target system for Buddy compression. We use a large NVLink-connected system memory or disaggregated memory pool for the buddy storage. The overall node organization is similar to that of an NVIDIA DGX-2 [19].

data movement to and from the GPU to stay within device memory limitations (adding algorithmic complexity) [7, 4, 8], or (iii) rely on off-GPU memory accesses or Unified Memory [9] to automatically oversubscribe device memory (limiting performance) [10, 11]. In this paper, we explore memory compression as a solution to this challenge.

Main memory compression has been studied in detail for CPUs [12, 13, 14, 15, 16]. While one can use the insights from previous work, GPU-specific workloads and architectural details pose very different trade-offs. The solutions in CPU solutions assume certain abilities that are difficult to achieve in GPUs. For instance, they assume compressed pages to be of different sizes, that can be re-allocated as the compression ratios change [13, 14, 15, 16]. Due to the immense device memory bandwidth, handling such on-the-fly page re-allocations is difficult and time consuming in GPUs [10].

Domain-specific hardware compression for graphics [17] and explicit compression in applications has been used in the past [18] to help with large workloads on GPUs. Hardware memory compression to increase memory capacity for general purpose applications in GPUs, however, remains unexplored.

We design Buddy compression, to utilize a larger-but-slower memory connected with a high-bandwidth interconnect as a fallback for incompressible data. Figure 1 shows an example system using Buddy compression. This design maintains a good compression ratio and high performance, while avoiding the complexity and performance concerns of mapping CPU memory compression approaches on GPUs. To summarize the research contributions of this work:

- We provide an in-depth analysis of the data of representative GPU workloads and derive insights to make GPU compression more effective.
- We introduce the first mechanism that uses general-purpose compression to increase the memory capacity of GPUs. Buddy compression is unique as compared to other compression solutions, since it does not require any additional data movement as the compressibility of the data changes.
- We evaluate the overheads of using Buddy compression across different interconnect-bandwidths and show that it is within 2% of the performance of an ideal, high-memory-capacity GPU.
- Finally, we show a case study on DL training to quantify the gains from using Buddy compression to increase the supported mini-batch size, and observe an average of 14% speedup in deep learning training workloads.

## 2. BACKGROUND

This section presents relevant concepts for modern GPU-based systems, it describes the state-of-the-art work in memory compression, and it presents the target applications for GPU memory compression.

### 2.1 Modern GPU Technologies

**Unified Memory.** Unified Memory, introduced in CUDA 8 for Pascal-class GPUs [9], shares a single memory space across a heterogeneous node. Non-local Unified Memory requests either remotely access data through the GPU interconnect or they result in transparent data migration with the placement of any piece of data being determined by a variety of heuristics [9, 20]. This feature proves helpful for programmers trying to communicate across GPUs. Unified Memory also supports memory over-subscription, meaning that Unified Memory-managed regions that are larger than the GPU device memory can be accessed without explicit data movement. This can greatly simplify the programming of large-memory jobs, but automated page migration has not proven performant enough to replace explicit data movement. Applications with large hot working sets experience frequent page faults and thrashing with Unified Memory, causing high performance overheads [20, 21, 22].

**High Bandwidth Interconnects.** There has been a natural drift towards scaling up to multi-GPU systems to address problem size growth. Multiple GPUs work on the same problem in parallel, occasionally communicating intermediate results or remotely accessing results through Unified Memory. Such communication tends to lie on the critical path for most solutions, making the interconnect between the GPUs very important. In recent years, high bandwidth interconnects like NVLink [23], openCAPI3.0 [24], and NVLink2 [19] have been used to alleviate this bottleneck. NVLink2 provides 25GBps of full-duplex unidirectional bandwidth per *brick*. Modern compute-class V100 GPUs support six NVLink2 bricks per GPU, offering a bidirectional bandwidth of up to 150GBps (full-duplex), much higher than the 16GBps  $\times$  16 PCIe3.0 full-duplex connection. The NVIDIA DGX-2 [19] workstation has sixteen V100 GPUs connected through an NVLink2 switch that supports the full 150GBps traffic

between any two GPUs. IBM Power9 CPUs also support six NVLink2 bricks, allowing high-speed remote access to system memory [25].

**Buddy Compression Target System.** Given these trends in modern GPU nodes, the future-facing system we envision for Buddy compression is shown in Figure 1. It is composed of NVSwitch-connected multi-GPU nodes with NVLink2-based access to a larger source of remote memory. This remote memory could be the system memory of a Power9 CPU, unused peer GPU memory, or an NVLink-connected disaggregated memory pool. While we know of no current NVLink-connected disaggregated memory appliance, such a device is a natural extension of the technology that is being explored for servers [26, 27]. Because all remote memory sources operate at the full NVLink2 bandwidth, Buddy compression applies equally well regardless of the source of the remote memory pool.

### 2.2 Memory Compression

For decades, memory compression in various forms has been proposed and used as a solution to the memory capacity challenge in CPUs. Most modern operating systems compress the swap space to reduce paging to disk [28, 29]. IBM MXT [12] was built with the purpose of solving the memory capacity challenge. Since then, there have been multiple academic research proposals for better hardware-accelerated main memory compression [13, 14, 15, 16]. There are several design choices and challenges that are addressed by each of these proposals. We now present these design points in brief.

**Compression Algorithms.** A hardware memory compression algorithm should be fast, require little energy, yet result in high compression rates. Several algorithms have been explored in past work [30, 31, 32, 33, 34]. We choose Bit-Plane Compression (BPC) [34] for Buddy compression. BPC is one of the latest algorithms in hardware memory compression and has been proven to have high compression ratios for GPU benchmarks when applied for DRAM bandwidth compression.

**Compression Granularity.** The unit of data that is compressed or decompressed together is called the compression granularity. A higher compression granularity requires less metadata and generally results in higher compression. On the other hand, a lower compression granularity does not require as many read-modify-write operations as a higher granularity compression might. Most previous main memory compression work uses a cache-block sized compression granularity. We also share this design decision, and, following the results of microbenchmarks [35], use a 128B size memory-entry to be the compression granularity for Buddy compression.

**A Typical Compressed DRAM Scheme.** When compressed, a unit of data can occupy different space in memory, depending on its compressibility. This requires special translation for such data. Within a page, different memory-entries can be of different sizes, requiring additional metadata to find the memory-entry offset in a compressed page. This metadata lookup generally lies on the critical path for every access to the memory.

The layout of a compressed main-memory is somewhat similar in all previous work on main memory compression in CPUs. There is some space dedicated for the compression

metadata, and the rest is arranged as variable-sized pages. Page size is decided by the compressibility of the data within a page.

**Compressed Data Movement and Allocation.** As data is written back to a compressed memory, value changes can lead to changing compressibility. This means that a memory entry can grow or shrink over time, leading to additional data movement [16]. This additional data movement makes the allocation choices very important, since, in an unoptimized setting, size-changes can lead to a domino effect of data movement within and across a page. Allocation granularity is closely related to the data movement overhead. For example, if each memory-entry in the memory is separately allocated, its size changes do not affect other data. However, if the allocation granularity is a page, a memory-entry size growth can lead to a domino-effect of data movement.

### 2.3 High-Throughput GPU Workloads

We briefly describe the target workloads for this work and the need for higher memory capacity in these workloads.

**HPC Workloads.** Several important HPC applications, ranging from fluid dynamics to weather prediction, have found GPUs to be the accelerator of choice. The sizes of the models and analyses in these applications have outgrown GPU device memory. Today, scientists use either Unified Memory or multiple GPUs to scale the models. Device memory compression can be very useful for such cases. We use a subset of SpecAccel2 and FastForward benchmarks to represent these HPC applications. The subset is chosen based on the confidence in the representativeness of the data values used in the benchmarks. All the discarded benchmarks seemed to have large portions of their working sets be zero, thereby having unrealistically high compression ratios.

**DL Workloads.** Training deep neural networks has become an important use-case for GPUs. As these networks grow deeper and wider, they require more data and are inevitably hitting the memory-capacity wall. Even the networks that do fit in GPU memory are unable to fit large enough batch-sizes in device to optimally utilize resources during training iterations [3], finally resorting to horizontal scaling that is not sustainable. Many domain-specific solutions across the stack have been proposed to deal with this memory capacity challenge in deep learning training [36, 37, 38, 39, 18, 5, 40, 8]. We use a set of convolutional neural networks (CNNs) and one recurrent neural network (RNN) to represent this class of workloads in our evaluation. Tab. 1 shows the memory footprints of our workloads.

## 3. GPU COMPRESSION CHALLENGES

Tab. 1: Details of the GPU Benchmarks Used

HPC SpecAccel	HPC FastForward
351.palm	2.89GB
352.ep	2.75GB
354.cg	1.23GB
355.seismic	2.83GB
356.sp	2.83GB
357.csp	1.44GB
360.ilbdc	1.94GB
370.bt	1.21MB
	FF_HPGMG-FV
	FF_Lulesh
	BigLSTM
	AlexNet
	Inception_V2
	SqueezeNetv1.1
	VGG16
	ResNet50
	2.32GB
	1.59GB
	2.71GB
	8.85GB
	3.21GB
	2.03GB
	11.08GB
	4.50GB

Graphics-specific compression has been used in GPUs for decades. The graphics pipeline of GPUs includes texture memory that is lossily compressed offline using tailored compression algorithms [17] in order to reduce the footprint of these textures. More recently, there are lossless online compression blocks for graphics workloads that save bandwidth (but not capacity) to and from main memory for some surfaces [41]. To our knowledge, compression is not currently used for compute workloads on GPUs. There are a number of compression challenges in GPUs that we address through design of Buddy compression.

**Page-Faulting Expense.** The immense parallelism of a GPU increases the throughput of work done. Driver-based page-fault handling, however, is remote and non-distributed, making GPU page-faults during the runtime of a kernel expensive. As data is written back to memory, its compressibility can reduce, requiring new page allocations to store the same data. The page fault overhead in GPUs makes decreasing the compressed data movement a very important directive.

**Metadata.** Memory bandwidth is another possible bottleneck for GPUs. Accordingly, there has been fruitful research on bandwidth compression of GPU main memory [34, 42]. Buddy compression uses compression to amplify *both* the bandwidth and capacity of GPU memory. However, as discussed earlier, compression-for-capacity requires additional metadata for translation into the compressed address space. This makes reducing the metadata size an especially important directive for our design.

**GPU Benchmark Compressibility.** In order to estimate the possible gains from compression, it is imperative to first find how compressible the high-footprint GPU workloads are. To this end, we take memory dumps of the workloads running on a Tesla P100 GPU with an Intel Xeon E5 host. We intercept each GPU *malloc* and *free* API call (including variants for pinned and Unified Memory-managed memory) to dynamically track the current allocated regions in the device memory. We divide the entire runtime of the workload into 10 regions, and at kernel boundaries of each region, take a memory dump of the allocated device memory.

Figure 2 shows the compression ratio of each benchmark using BPC compression [34] over its entire run. Note that these compression ratios are quite optimistic capacity compression, since they assume eight different compressed memory-entry sizes are available (0B, 8B, 16B, 32B, 64B, 80B, 96B, and 128B) and assume no page-packing overheads. That is, each memory-entry is individually compressed and allowed to occupy any of the above mentioned sizes. On average, the geometric mean of compression ratio for the HPC workloads is 2.51 for the HPC benchmarks and 1.85 for the DL benchmarks. This is a higher average as compared to prior work on CPU workloads [16], and can be attributed to the higher percentage of homogenous data allocations (with a single uniform datatype). Prior work has established that Bit-Plane Compression works well for homogenous data, and such homogeneity is prevalent in GPU workloads [34].

**Compressibility Changes.** As compared to previously studied workloads [14, 16, 13], the compressibility over time changes more often in GPU benchmarks. The most extreme example is 355.seismic, which begins with many zero values but slowly asymptotes to a 2x compression ratio over its

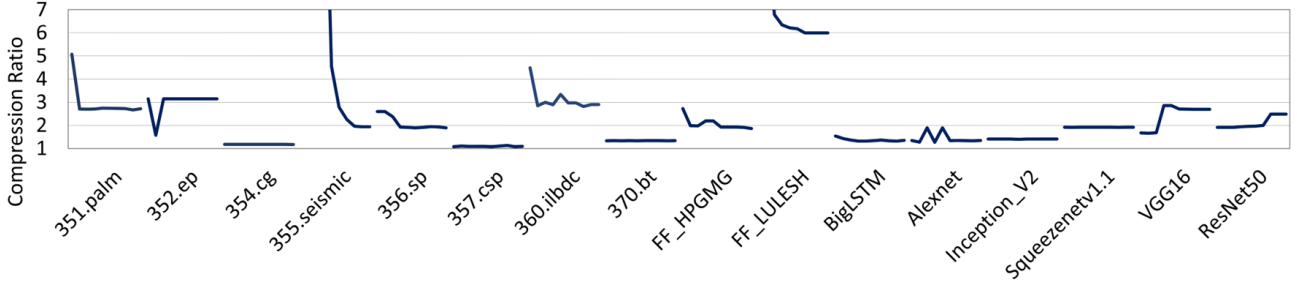


Fig. 2: The average compression ratio for the entire memory footprint of each program.

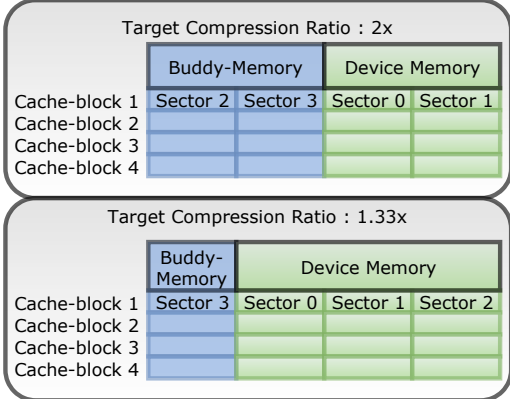


Fig. 3: The layout of a compressed 128B memory entry using Buddy compression. Each 32B sector is stored in NVLink-connected buddy-memory only if the target compression ratio is not met.

execution. We also observe that although the overall compression ratio of the DL workloads stays roughly constant, there are frequent compressibility changes for individual memory entries. This is likely due to the fact that DL frameworks perform their own asynchronous GPU memory allocation with software-managed memory pools, and may reuse the same memory location for a variety of purposes over program execution [43]. In some cases, the data in a memory-entry can grow more random over time, thereby decreasing its compressibility. This would require more space to be allocated for the same memory-entry, causing a *memory-entry overflow*, and thereby additional data movement, as discussed in Section 2.2.

## 4. BUDDY COMPRESSION

Having observed the opportunity for compression, and established the basic differences in the requirements in GPUs as compared to CPUs, we define the goals of Buddy compression. The main design goals for this work are to compress the GPU device memory for additional capacity large-footprint workloads, such that (i) we do not impact small-footprint workloads that currently fit in GPU memory (ii) data movement due to changes in compression is small, and (iii) the complexity of allocation and translation for compression is low.

### 4.1 Buddy Compression Overview

Buddy compression allows a programmer or DL framework to annotate memory allocations such that they take up less device memory than the allocation size. For instance, if a user has 24GB of data but a GPU with only 12GB of memory capacity, the data can be allocated targeting 2x compression. This means that only 1/2 the of the full data size

is allocated on the GPU, and the allocations fit in device memory. We use compression to opportunistically fit data into this reduced device-resident allocation, while an NVLink-connected larger memory is available as overflow storage for uncompressible data. The *buddy memory* is used as extended storage at 128B memory-entry granularity. Data from compressible memory-entries is sourced completely from GPU device memory, while incompressible memory-entries are sourced from both device and buddy memory.

As shown in Figure 3, Buddy compression stripes the data at a 32B sector granularity across device memory and system memory based on the target compression ratio of an allocation. This 32B sector size is chosen to match the access granularity of GPU memory<sup>1</sup>. For example, if an allocation targets a compression ratio of 2x, the first two sectors per 128B memory-entry are mapped to the device memory, while the last two are mapped to the system memory. Therefore, as long as a memory-entry can be compressed to 2x or more, it fits completely on the device memory. However, if the data is not as compressible as expected in this particular memory-entry, then, the rest of its data is saved in its fixed, pre-allocated spot in the buddy memory.

At boot time, the host system carves out a physically-contiguous chunk of its memory for each GPU, dedicating this storage to be used as each GPU's buddy memory. This carve-out is then never accessed by the host, eliminating any coherence issues. The buddy memory size should correspond to the maximum target compression ratio for the GPU. As an example, if the maximum target compression ratio is 4x, then the carve-out should be 3x as large as GPU's device memory, in order to allow each memory-entry to have 3 sectors in host (in the worst case) and only 1 on the GPU.

The use of buddy memory for uncompressible data solves both of our design goals. *The goodness of the design lies in the fact that the compressibility of each memory-entry affects only its own allocation, thereby never having to cause page movement*. Additionally, since the carve-out is a contiguous region in the host memory, addressing into the buddy memory is offset-based and trivial. The additional metadata for compression includes: (i) the target compression ratio, which is held in the page table entries, and (ii) whether accessing the data requires a read to the buddy-memory, which is a fine-grained metadata at a memory-entry granularity. The fine-grained compression metadata is stored in a dedicated driver-managed region of device memory, with a small overhead of 0.4% (4 bits per 128B memory-entry). The overall translation mechanism is simple, since there is no translation required for

<sup>1</sup>Specifically a 32B access granularity applies to GDDR5, GDDR5X, GDDR6, and HBM2-based GPUs.

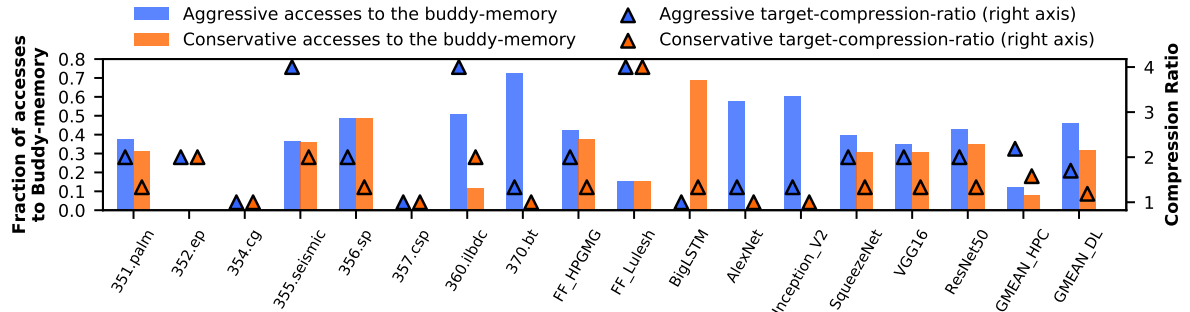


Fig. 4: The fraction of memory accesses that require buddy memory access over NVLink using a whole-program compression target.

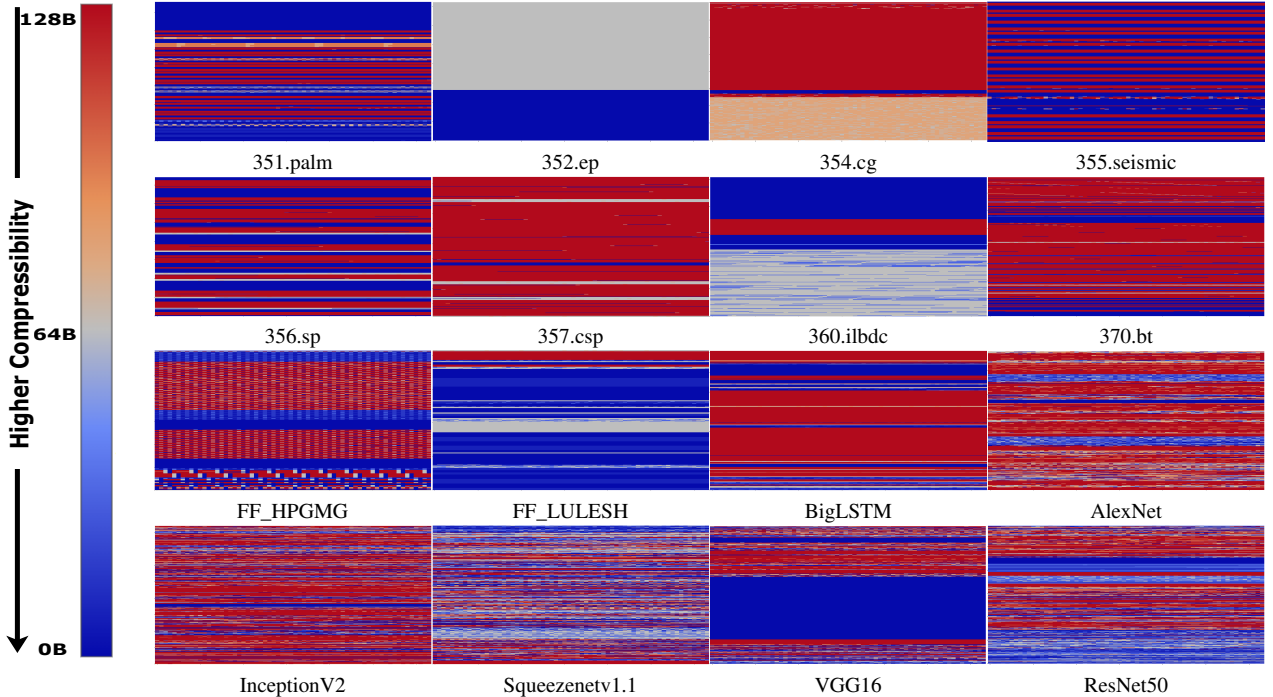


Fig. 5: Spatial patterns of compressibility. Each plot shows a heatmap of the compressibility for the total allocated virtual address space for each program. The virtual address space is shown in increasing order, with a pixel representing a single 128B compressed memory entry. Pixels for 64 128B entries are stacked horizontally, making one horizontal line an 8KB page. Pages are then stacked vertically in increasing order of virtual address.

the device memory address apart from modifying the memory entry offset within the page based on its compression ratio. We further discuss the metadata and translation in Section 4.3.

## 4.2 Understanding and Reducing Buddy Compression Overheads

With the design of Buddy compression, the obvious overhead comes from having to access the slower buddy-memory in cases of unexpectedly low compression. The choice of a target compression ratio is important, since aggressive compression ratios will lead to higher number of lines exceeding the allocated device memory and requiring buddy-memory accesses. To choose the target compression ratio, we assume that either expert domain knowledge or profiling data are available. In this paper, we use a profiling pass of each benchmark to represent such knowledge.

The granularity with which the programmer annotates memory is also important—the best annotation granularity depends on the spatial characteristics of compressibility. Below, we first consider a single target compression ratio for the

whole-program, finding it to be too coarse to effectively get high compression ratios without frequent buddy memory accesses. We then present a study of the spatial characteristics of data compressibility, finding good locality for individual memory allocations. Per-allocation target compression ratios both increase the overall compression ratio, and substantially decrease the buddy memory traffic. Finally, based on the spatial study of compressibility, we also present a compression optimization that targets mostly-zero memory allocations.

### 4.2.1 Whole-Program Compression Targets

Figure 4 shows the fraction of memory accesses that require an access to buddy memory using whole-program compression targets. The allowed compression ratios for this study are only 1x, 1.33x, 2x and 4x. These ratios are chosen to keep the sector interleaving simple and avoid unaligned sector accesses. With aggressive target compression ratios (judged through profiling), we achieve an overall compression ratio of 2.18x for HPC workloads, and 1.7x for DL workloads. However, it leads to a 12% accesses

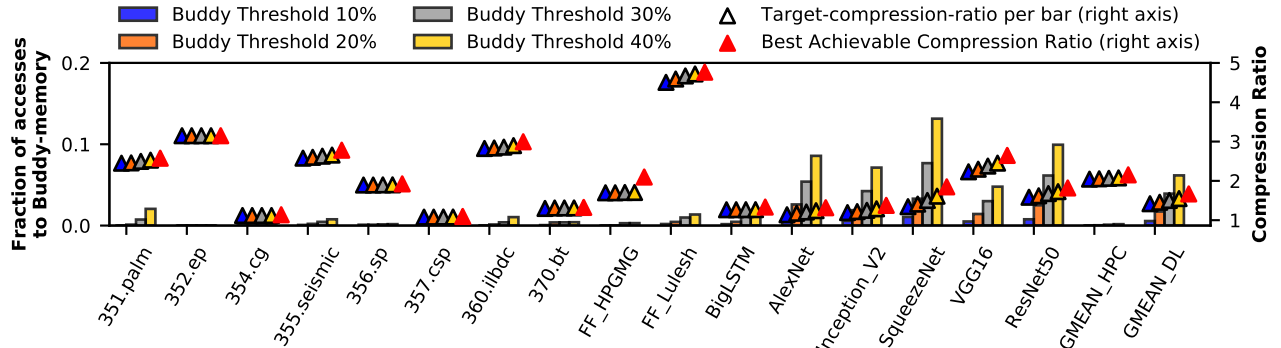


Fig. 6: Sensitivity of the compression ratio and buddy-memory accesses to the Buddy Threshold parameter.

over the interconnect to the buddy-memory for HPC, and 46% for DL. Given that even the highest available bandwidth on the interconnect (NVLink2, 150GBps) is 6x lower than the GPU device memory bandwidth (900GBps), the overheads from these buddy-memory accesses would be high.

One simple solution could be to choose a conservative target compression ratio to lower the overheads. As the figure shows, such a solution would bring down the buddy-memory accesses to 8% and 32% respectively for the HPC and DL workloads. These percentages are still high, and come at a cost of lower compression. The overall compression ratios are now merely 1.57x and 1.18x for HPC and DL respectively.

The desirable solution for us would be something that effectively lowers the buddy-memory accesses, while maintaining high compression ratios. In order to find such a solution, we present a deep dive into the detailed compression data patterns in these workloads.

#### 4.2.2 Understanding Compressibility Patterns

Figure 5 shows a spatial plot (in the virtual address space) of the compressibility of each workload’s data. Each sub-plot is a spatial heat map that shows the compressibility of each 128B memory-entry in the memory allocated by each benchmark. A colder color, like blue, signifies high compressibility, and hotter colors like red show low compressibility. The plot is structured assuming 8KB pages, where each page has 64 128B memory-entries, laid along x – axis. The y – axis is therefore the total number of pages in the memory of the benchmark. Figure 5 shows that the spatial locality of compressibility of data is highly varied across benchmarks. While most HPC benchmarks have large homogenous regions of similar compressibility, the trends are more random in DL workloads. FF\_HPGMG shows specific patterns of compressibility that can directly be correlated with the arrays of heterogeneous structs that are used in its allocation. Although the DL workloads do not show the level of homogeneity that can be seen in HPC workloads, there are still faint patterns that show few mostly-red and mostly-blue regions in a majority of them. Based on the insights from these plots, we propose optimizations to the design of Buddy compression.

#### 4.2.3 Per-Allocation Compression Targets

Previously, we considered a single target compression ratio for the entire memory footprint. However, the Figure 5 shows that there are several regions that are mostly-red, or mostly-blue. Upon investigation, majority of these region-boundaries

overlap with cudamalloc() boundaries. A special allocation API for compressed regions can allow us to capture this behavior and eliminate the futile effort of compressing the red regions. Our original profiling pass with a smaller dataset can be augmented with some additional profiling information to enable such an allocation-level decision-making.

To simplify profiling, we use a static, representative snapshot of memory, to output static target compression ratios per allocation. A representative snapshot is defined as a point in execution when the compressibility is a conservative, near-average value of the full run. As an example, based on Figure 2, for 355.seismic, the snapshot used will be the one with compression ratio 2x, and not the ones with a 7x or 6x compression ratio. We use a static target, because a dynamic target compression ratio would require reallocating and moving around the pages, making the compression management more complicated and less performant.

Most benchmarks have regions that are highly homogeneous in their compressibility, making the per-allocation target ratio decision simple. However, for benchmarks like AlexNet and ResNet50, the regions are mixed in compressibility. Therefore, target compression ratio decision in these cases, involves a trade-off between compression ratio and buddy-memory accesses. We define a *Buddy Threshold*, that sets a limit on the fraction of memory-entries that require accessing the buddy-memory, per-allocation. A higher Buddy Threshold will help us achieve a higher compression ratio at the cost of more buddy-memory accesses, and hence, lower performance. These buddy-memory accesses are calculated per target compression ratio, using a histogram of the static memory snapshots.

Figure 6 shows the results from a sensitivity study of the Buddy Threshold. For Buddy Threshold, we sweep the range from 10% to 40%. In addition to this, the figure shows the best achievable compression ratio assuming no constraints are placed on the buddy-memory accesses. The bars in the figure show that the buddy-memory accesses remain very low for HPC benchmarks, due to their homogenous regions. For DL benchmarks however, the buddy-memory accesses are comparatively higher, and increase further as the buddy threshold is increased. Similarly, the compression benefits from increasing the buddy threshold are mostly seen in DL benchmarks.

With the exception of FF\_HPGMG, we are able to achieve almost-optimal compression, as can be seen in comparison with the black marker. FF\_HPGMG, as discussed earlier has a peculiar striped compressibility pattern that is attributed to

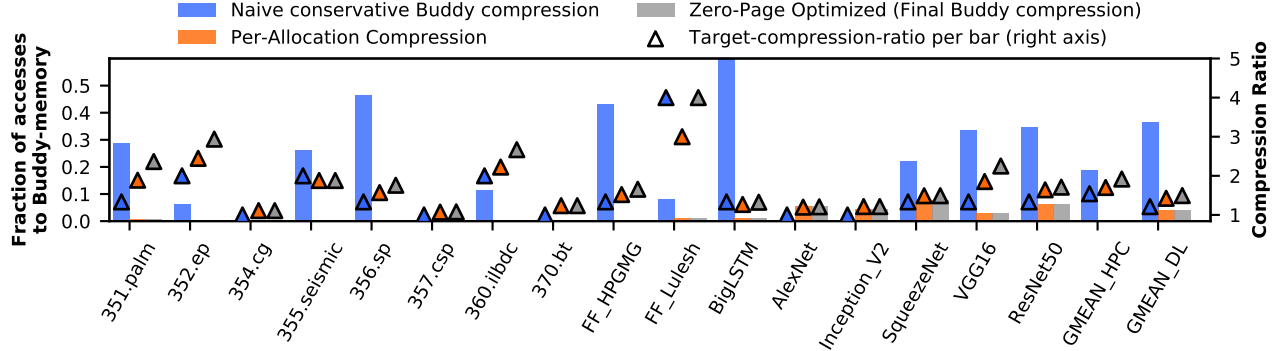


Fig. 7: Sensitivity of the compression ratio and buddy-memory accesses to design optimizations.

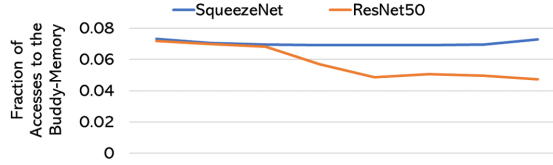


Fig. 8: The fraction of buddy storage accesses over the execution of one iteration in DL training. We achieve a constant compression ratio of 1.49 for SqueezeNet and 1.64 for Resnet.

the struct it uses. In order to capture the maximum compression, FF\_HPGMG requires more than 80% Buddy Threshold for most of its allocated memory region. Another interesting scenario is seen in benchmarks 354.cg and 370.bt. Since these benchmarks mostly comprise of incompressible data, without the per-allocation targets, Buddy compression was unable to compress them at all. However, with the per-allocation targets, we are able to compress them to 1.1x and 1.3x respectively. Overall, since a 30% Buddy Threshold achieves a good balance between the compression and buddy-memory accesses, we choose this for our final Buddy compression design.

Since the target compression ratio remains constant, while actual data compressibility can change over time, these statistically calculated buddy-memory accesses may not be similar across the run. In order to investigate this, we observed the buddy-memory accesses across all the memory dumps, while maintaining constant target compression ratios. In Figure 8, we present the results from ResNet50 and SqueezeNet, both of which have frequent changes in compression ratio per memory-entry, and have high accesses to buddy-memory to begin with. We observe that the buddy-memory accesses do not change a lot over time. This is because even though the individual memory-entries frequently change their compressibility, the changes are almost equally in both the directions, making the overall effects small. Furthermore, as mentioned earlier, for benchmarks that see large changes in their overall compressibility, like 355.seismic, we avoid this challenge by choosing conservative target compression ratios.

#### 4.2.4 Special Case For Mostly-Zero Allocations

Based on the spatial plots, we observe that there are areas in memory that remain mostly-zero during complete benchmark execution. To capture the capacity-expanding opportunity of such allocations, we add a very aggressive target compression ratio of 16x where we keep only 8B out of each 128B on the device memory. Note that the only change involved here is

an additional encoding for page size in the TLB.

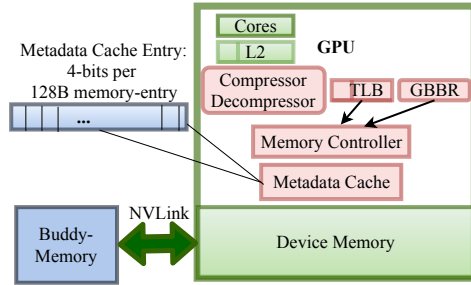
This optimization allows us to increase the compression ratio for benchmarks with large blue regions, for example, 352.ep, and VGG16. Note that this optimization does not have much impact on the buddy-memory accesses, since such compressible data would always fit in device memory. Figure 7 shows the impact of this optimization. For HPC benchmarks, the compression ratio goes up from 1.7x to 1.9x, while for DL, from 1.42x to 1.5x.

This is an aggressive optimization, where it is important to identify allocations that are not only mostly zero, but also remain so for the entirety of the run of the benchmark. The profiler needs to carefully mark the regions that can be compressed with this optimization, such that the overall compression ratio is still under 4x, to match the buddy-memory reserved area. If the prediction goes wrong, the program could crash, just like it would, even if compression was not used. We therefore separate the results in Figure 7 between the two optimizations, showing that skipping this optimization in most cases does not lead much loss in compression, and has no discernable impact on the buddy-memory accesses. Later, in Section 7, we discuss how Unified Memory can help us achieve even more aggressive compression.

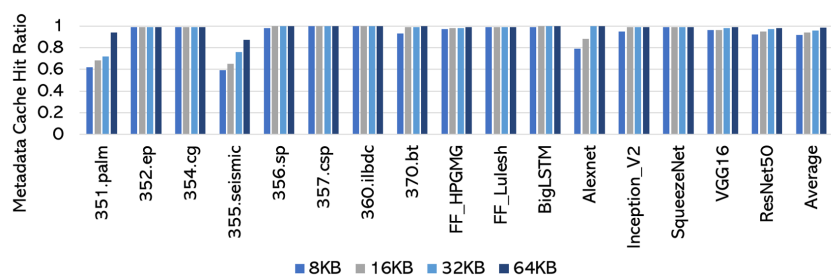
### 4.3 Architectural Changes

Once the data is stored in a compressed form, addressing it requires some additional translation and metadata. This metadata informs us about (i) the target compression ratio, (ii) whether or not a particular memory-entry was compressed to the target ratio, and (iii) the address in buddy-memory to be accessed for memory-entries that did not compress to the target ratio.

A global base address for the buddy-memory's carved out region is known to the system in GBBR (Global Buddy Base-address Register). The page-table and TLB are extended to store the information about whether the page is compressed or not, the target compression ratio, and the offset of buddy-page from the global base address. This adds a total overhead of 24 bits per page-table entry. In order to know the compressed size of each 128B memory entry, there is 4-bits of metadata per cache block, stored in a dedicated region of device memory, amounting to a 0.4% overhead in storage. The metadata storage overheads of Buddy compression are either comparable to, or less than the various previous works in memory compression in CPUs [16, 14, 12, 13, 15]. Figure 9a shows



(a) High-level overview of architectural changes/additions with Buddy compression.



(b) Metadata cache hit rates with different sizes of total metadata cache

Fig. 9: Compression metadata handling and architecture

a very high-level view of the metadata setup and translation.

A metadata cache is used to avoid additional memory accesses each time the memory is accessed. Figure 9b shows the metadata cache hit ratios as a function of the metadata cache size. Most applications have high hit ratios. We use a 4-way 32KB metadata cache, that is split into 8 slices, 1 per frame-buffer partition, or FBP. Each metadata cache entry is 32B, thereby causing a prefetch of metadata corresponding 63 neighbor 128B memory-entries upon every metadata cache miss. The metadata is assumed to be interleaved across the FBPs using the same hashing mechanism as regular physical addresses interleaving.

Buddy compression has a metadata-related benefit, in the form of less strict metadata and data access ordering. Upon a metadata cache miss, the device-memory data, and its metadata can be accessed in parallel, since the metadata only informs us about the buddy-memory part of data, not the device-memory part of it. We do not, however access the buddy-memory in parallel, since the buddy-memory accesses are very low on average, ad seen in Figure 7.

#### 4.4 Final Design

Buddy compression uses a Buddy Threshold default of 30%, a metadata cache of 4KB per frame-buffer partition (or, channel), and a buddy-memory of size 3x of the GPU device memory, to support a 4x maximum compression ratio. The final flow of compression selection looks like this: (1) The application is executed in profile mode with a smaller, but representative dataset. (2) During the profiling, our tool periodically calculates a histogram of compressed memory-entries per allocation. (3) Once the run is complete, the tool calculates the target compression ratio by looking at the compression over time per allocation. (4) These target compression ratios are then saved as profile output. The programmer can then use these target compression ratios as a directive, to be used with the special cudamalloc APIs, and run a larger dataset without the overheads of Unified Memory.

Figure 7 shows the compression ratio and buddy-memory accesses for the final design. We achieve 1.9x compression for HPC and 1.5x compression for DL workloads. The average buddy-memory accesses are 0.08% for HPC and 4% for DL workloads. We now present the performance evaluation of Buddy compression.

### 5. METHODOLOGY

Before presenting results we briefly describe our experimental methodology.

#### 5.1 Workloads

As previously described, we evaluate Buddy compression's effectiveness on workloads from the SpecAccel [44] and Fast-Forward benchmark suites for HPC workloads. We collect a representative trace from each benchmark while running the reference datasets. Each trace contains 1–9 billion warp instructions and corresponds to the dominant kernel of each benchmark at a point in execution that exhibits the average compression ratio for that entire benchmark execution. We also consider a set of 5 convolutional neural networks: AlexNet [45], Inception v2 [46], SqueezeNetv1.1 [47], VGG16 [48], and ResNet50 [49], all of which were run under the Caffe [43] framework with the ImageNet [50] dataset. Additionally we consider a long short-term memory network, BigLSTM [51], which is a 2-layer LSTM with 8192+1024 dimensional recurrent state in each of the layers. This network uses the English language model. The trace for each of these DL training workloads spans one full iteration, including both forward and backward propagation.

#### 5.2 Simulation Infrastructure

We employ two performance simulators to evaluate the impact of Buddy compression. The first is a trace-driven GPU performance simulator, similar to the one used by Arunkumar et al. and others [52, 53, 54]. We configure the simulator based on publicly information about NVIDIA's P100 Pascal GPU [55] and the interconnect characteristics of recent Volta GPUs [56] (Tab. 2). Non-public microarchitectural details are configured using microbenchmark results from Jia et al. [35]. Each SM is modeled as an in-order processor with greedy-then-oldest warp scheduling. We model a multi-level cache hierarchy with private L1 caches and a shared sectored L2 cache with 128B lines and 32B sectors. Caches are banked to provide the necessary parallelism to saturate DRAM bandwidth. We model software-based cache coherence in the private caches, similar to state-of-the-art GPUs. The memory system consists of 32 HBM2 channels and the GPU is connected to the system with 6 NVLink2 bricks. We extensively validated the simulator and its event counters and performance characteristics are highly correlated to recent NVIDIA GPU designs.

We conservatively model decompression latency as 11 DRAM cycles, as discussed in prior work [34]. Unless explicitly noted, the default metadata cache configuration is 4-way set associative 4KB per L2 slice. Additionally, to separate out its performance impact, we also evaluate bandwidth-only interconnect compression between the L2 cache and device memory. Such compression does not

**Tab. 2: Performance simulation parameters.**

Core	1.3 GHz; 2 greedy-then-oldest warp schedulers per SM Max 64 32-thread warps per SM
Caches	24KB private L1/texture cache per SM, 128B lines 64KB dedicated scratchpad per SM, 4MB shared L2, 32 slices, 128B lines, 16 ways
Off-Chip	32 HBM2 channels at 875MHz (900 GBps) 6 NVLink2 bricks (150 GBps full-duplex*)
Buddy	4KB* metadata cache per L2 slice, 128B lines, 4 ways Compression/Decompression latency = +11 cycles

\* These parameters are swept in later parts of the evaluation.

increase the effective memory capacity, but it can increase the bandwidth between L2 cache and memory without requiring any metadata or buddy-memory accesses.

Our second simulator is designed specifically for deep neural networks and we use it to evaluate the benefits of the larger mini-batches enabled by Buddy compression (Sec. 6.2.2). We use this proprietary simulator because we cannot collect traces for DL execution with memory capacity needs that are larger than current GPU’s capacity. This simulator, similar to Paleo [57], uses analytical models to project DL processing throughput as workload and architectural parameters are varied. We extensively validated the simulator and its projections are highly correlated with a range of existing commercial GPUs.

## 6. PERFORMANCE EVALUATION

We have already presented results regarding buddy-memory accesses and compression ratios from Buddy compression in Figure 7. In this section, we first discuss the performance impact of Buddy compression relative to an ideal infinite-capacity GPU. We then present a case-study of DL training to estimate the performance benefits from increased capacity.

### 6.1 Performance Relative to an Ideal GPU

Apart from increasing the memory capacity, Buddy compression can affect the performance of the system in the following ways: (i) It has two conflicting effects on the effective bandwidth from L2 cache to device memory. First, since compression is done at the cache-block granularity, the minimum L2 fill granularity is no longer a single 32B sector. Instead, the complete cache-block is transferred to L2 upon a load access to a compressed memory-entry. This may result in over-fetch for fine-grained accesses, squandering device memory bandwidth. However, for compressible workloads with high locality, compression allows an increase in effective bandwidth because cache-blocks can be fetched with fewer memory accesses. (ii) Metadata cache misses can cause additional requests to device memory. (iii) Decompression latency can lead to slower performance. (iv) Buddy-memory accesses can cause a performance hit.

We evaluate Buddy compression alongside bandwidth-only compression that compresses the data being transferred between L2 cache and device memory. We also sweep the buddy-memory interconnect bandwidth from 50 to 200GBps on full-duplex connection, where 150GBps represents NVLink2.

The results are shown in Figure 10. Bandwidth-only compression achieves an overall speedup of 5.5%. Most of

this speedup comes from the DL training workloads. This can be attributed to the regular, streaming memory accesses of these workloads, which are essentially performing matrix multiplications. Since most of their memory accesses are coalesced to access all sectors in each cache-block, bandwidth compression achieves higher effective bandwidth by requiring fewer packets per request. On the other hand, the HPC applications 354.cg and 360.ilbdc experience slowdowns with bandwidth compression. This is because of the random and irregular memory access pattern of these benchmarks. Most of their memory accesses require only one sector. However, bandwidth compression leads to a full cache-block transfer upon every memory access, leading to lower effective bandwidth. FF\_Lulesh experiences a slowdown despite having a regular memory access pattern. Upon investigation, we found the reason behind this to be the compression and decompression latency, that both lie on the critical path for bandwidth compression.

Buddy compression introduces additional overheads on top of bandwidth compression, in the form of metadata cache misses and buddy-memory accesses. Figure 10 shows that while an interconnect bandwidth of 200GBps still achieves a 2% average speedup using Buddy compression, all lower interconnect bandwidths experience some slowdown relative to the ideal infinite-capacity GPU that serves as the baseline. Note that the performance benefits from a larger memory capacity are not accounted for in these experiments.

The benchmarks 351.palm and 355.seismic experience slowdown due to a higher metadata cache miss rate, as can be seen from Figure 9b. Since the other benchmarks have high metadata cache hit rates, metadata accesses do not have a discernable impact on their performance.

Most HPC benchmarks have very low buddy-memory accesses (Figure 7), leading to negligible slowdowns with a high bandwidth interconnect. However, when the interconnect bandwidth goes down, even these 1% accesses from buddy-memory can cause a considerable slowdown in bandwidth-sensitive applications like 352.ep and 355.seismic. Note that FF\_HPGMG has host-memory accesses in its native form, due to synchronous copies from host to device. Therefore, lowering the link bandwidth shows drastic impact on its performance.

DL training workloads have a higher percentage of buddy-memory accesses, as can be seen in Figure 7. These buddy-memory accesses are caused by a lack of compression locality in the workloads. For example, AlexNet requires accesses to 5.4% of memory locations to go to buddy memory, leading to a 6.5% slowdown relative to ideal (with a 150GBps full-duplex interconnect). This is because of the difference in the bandwidth available from device memory vs buddy-memory, which in our setup is 900GBps and 150GBps. Performance degenerates quickly as this disparity grows, with the 50GBps full-duplex connection seeing a 35% slowdown.

These results show the recently-developed high-speed GPU interconnects to be an enabling technology for Buddy compression. The slowest link we evaluate (50 GBps full-duplex) is still faster than the most recent PCIe generation (x16 PCIe4.0, providing 32GBps full-duplex bandwidth) yet it suffers from more than 20% average slowdown relative to the ideal GPU. However, using high bandwidth interconnects

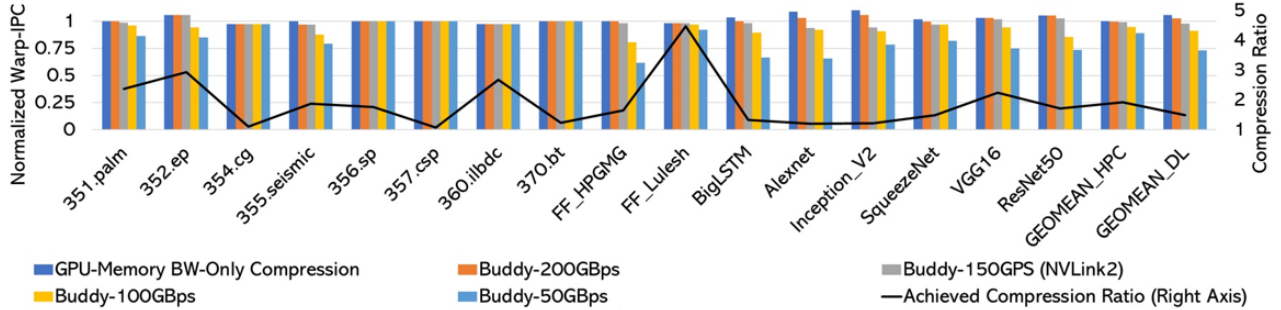


Fig. 10: The performance impact of compression, not accounting for capacity benefits. Buddy compression is evaluated with different link bandwidths (showing unidirectional full-duplex bandwidths). Results are normalized to a system with unlimited device memory and a 150GBps host interconnect.

such as NVLink2 (150Gbps full-duplex) enables Buddy compression to approach within 1% of the performance of the infinite-capacity GPU on HPC benchmarks, and within 2.2% of ideal on DL training workloads.

## 6.2 Case-study: DL Training Benefits from Increased Memory Capacity

Thus far, we have compared the performance of Buddy compression to an uncompressed, infinite-memory baseline (Figure 10). This excludes the benefits that benchmarks can achieve by having access to a larger-memory, thereby ignoring the main purpose of Buddy compression. In the case of HPC benchmarks, a larger memory enables solving a larger problem. Such benefits are important yet difficult to quantify. Accordingly, we instead perform a case-study on DL training workloads to quantify the performance benefits from compression.

The Stochastic Gradient Descent (SGD) method is widely used to update weight values during DL network training. SGD iterates repeatedly through the training dataset, optimizing and updating the model each iteration. Updates depend on hyperparameters (such as the chosen learning rate) and dynamically react as the classification accuracy increases. Since the datasets tend to be huge (ImageNet [50] has 1.2 million images), the entire dataset is divided into mini-batches. Each training iteration, therefore, goes through one mini-batch and updates the model. One run through the entire dataset is called an epoch, and consists of several thousand iterations in the case of CNNs that are trained on the ImageNet dataset.

### 6.2.1 Memory Footprints of DL Workloads

The memory footprint of a network during training depends on the mini-batch size being used. Larger mini-batch sizes require a larger part of the dataset to reside in device memory, along with more intermediate data (activations and gradients).

Figure 11a shows the memory footprint of each of our DL training workloads as the mini-batch size is increased. The sizes are increased up to the maximum size that a Titan Xp GPU (12GB device memory) can support. As is clear from the figure, initially there is not much difference as the batch size is doubled. Eventually, however, the memory footprint grows almost linearly with increasing mini-batch size. This transition point depends on the size of the network parameters, which do not vary with mini-batch size. For example, for AlexNet, the network parameters are a large portion of the overall memory consumption due to the three large fully-connected layers and relatively few (five) convolutional

layers. This leads to a later transition point for AlexNet at a batch-size of 96; all other tested networks transition to an increasing memory footprint at a batch size of 32 or below.

### 6.2.2 Performance Impact of Larger Mini-Batch

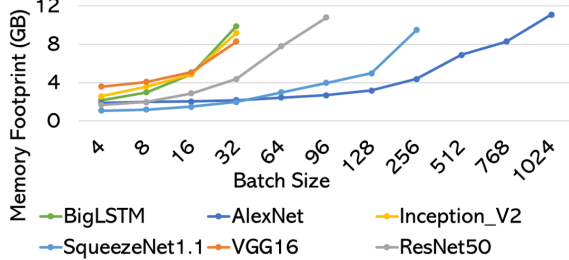
A larger batch size is beneficial for DL training [51, 3], because it allows more work to be done per iteration, leading to higher resource utilization. Figure 11b shows the projected speedup for each network as the mini-batch size is increased. It is generated using a detailed analytical model of deep learning training efficiency (Section 5). As shown in the figure, increasing mini-batch size leads to higher speed in terms of frames per second. This effect, however, is only seen until the mini-batch size is large enough to utilize most of the GPU resources. After the point of full GPU utilization, the effect plateaus.

Buddy compression can allow us to fit in a larger mini-batch into GPU memory. Figure 11c shows the relative speedup projected by our model for this larger mini-batch size over a baseline GPU with 12GB of device memory. The average speedup is 14%, while individual workloads like BigLSTM and VGG16 achieve high speedups of 28% and 30%, respectively. The reason for a higher speedup in these workloads follows from Figures 11a and 11b. Without compression, both of these are unable to fit the mini-batch size of 64, which allows a close-to-maximum resource utilization.

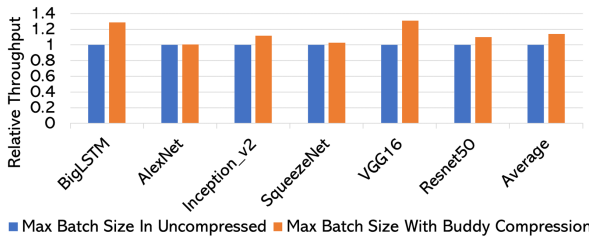
Note that this overall speedup of 14% is much higher than the 2.2% slowdown relative to an infinite-capacity GPU that was observed due to the Buddy compression overheads in Figure 10. This indicates that Buddy compression can lead to significant performance gains for capacity-constrained GPUs by allowing the use of larger mini-batch sizes.

### 6.2.3 Faster Convergence with Larger Mini-Batches

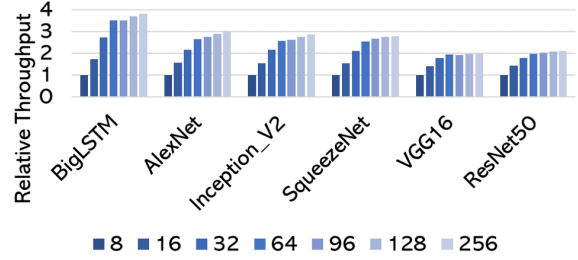
Apart from the effect on computational throughput due to resource utilization, the mini-batch size can also impact the training accuracy. In order to investigate this, we train ResNet50 on CIFAR100 [58] dataset for 100 epochs on a Titan Xp GPU with different mini-batch sizes. Figure 11d shows the validation accuracy results for these runs. As can be seen, very small mini-batches of 16 and 32 do not reach the maximum accuracy, despite using the corresponding hyperparameters. Additionally, although the mini-batch size of 64 trains to the maximum accuracy, it converges slower than the larger mini-batches. With batch normalization, the jitter in the accuracy is also higher with small mini-batch sizes. While we observe good validation accuracy up to a



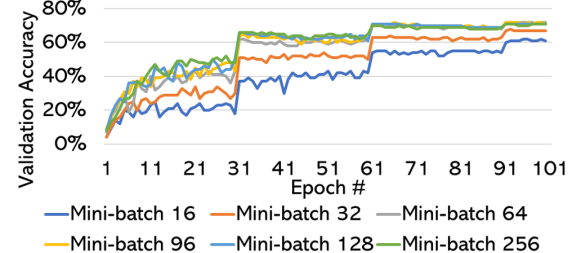
(a) Memory footprint of DL workloads as a function of batch size. PyTorch-based network models were run on a Titan Xp GPU.



(c) Projected speedup in images per second by using Buddy compression to achieve a larger batch size.



(b) Projected speedup in images per second as a function of mini-batch size.



(d) Validation accuracy with different mini-batch sizes. ResNet50 is trained until 100 epochs with CIFAR100.

Fig. 11: Impact of increasing mini-batch size on DL training workloads.

batch size of 256, it has been reported that increasing the mini-batch beyond a certain size can be detrimental to the network’s generalization. However, there has been work on tuning loss functions and hyperparameters for successful training with large mini-batches [59, 60].

Ultimately, the takeaway from this case-study is that most DL networks require a mini-batch of at least 64 or 128 in order to achieve near-maximum throughput and best accuracy, and Buddy compression can help achieve large mini-batch sizes for large networks using fewer GPUs.

## 7. DISCUSSION AND FUTURE WORK

**NVIDIA Unified Memory (UM).** Faithfully comparing the performance of Buddy compression to Unified memory in simulation is not feasible due to the complex host driver interactions and page migration policies implemented within UVM. Instead we chose to understand Unified Memory performance in oversubscription scenarios on real hardware. We performed experiments on an IBM Power9 system, connected to a Tesla V100 GPU via NVLink2 which provides 75 GBps full-duplex bandwidth to and from the CPU. We used the SpecAccel applications with the *managed* PGI compiler flag, to force the use of Unified Memory. Our results indicate that the migration heuristics for UM often perform worse than running applications completely pinned in host memory; perhaps because UM was primarily intended for the ease of programming and has not yet been tuned for high-performance memory oversubscription. Previous work [20, 10] supports our observation that the slowdown due to UM oversubscription can easily exceed 2–3x in many cases. This strongly suggesting that Buddy compression may be a better alternative to high performance memory over subscription than software based Unified Memory.

Additionally, it may be possible to apply Buddy compression alongside UM oversubscription to both improve performance and boost capacity further. Under UM, Migration of Buddy compressed pages will consume a smaller fraction of NVLink traffic than uncompressed pages, in turn reducing the cost of UM oversubscription. Moreover, if the programmer or Buddy compression runtime system is able to assume Unified Memory oversubscription can preserve functionality in all cases, then incorrect predictions due to aggressive Buddy compression optimizations (Section 4.2.4) will never lead to out-of-memory errors. This would enable improved dynamic and transparent runtime support for choosing the best Buddy compression target ratio.

**Other Capacity-Expanding Strategies.** An area of future work to explore is using Buddy compression in conjunction with domain-specific solutions for GPU capacity expansion. For instance, vDNN [38] proposes running large DL networks using manual offloading of data layer-by-layer. However, there are still cases where it fails, due to the inability to fit data required for just one layer [22]. Buddy compression can enable running larger networks with vDNN. Similarly, Buddy compression could be used in conjunction with other strategies like checkpointing [37] and Gist [18], where the performance-to-capacity trade-offs would be improved.

## 8. CONCLUSIONS

This work proposes and evaluates a novel GPU memory compression scheme called Buddy compression. Buddy compression is the first general-purpose mechanism that can be used to increase user visible GPU memory capacity on GPUs. Buddy compression works by targeting specific compression ratios and maintaining compressed data within GPU memory when compression targets can be achieved,

while spilling uncompressable data into system memory, peer GPU memory, or other pools of disaggregated memory accessible over high speed inter-GPU interconnects. Buddy compression is able to achieve memory compression ratios between 1.5–1.9× across a wide range of HPC and deep learning workloads while incurring only a 2% performance penalty compared to a system with equivalent GPU memory capacity. This combination of high performance and reasonable compression ratios is likely to make Buddy compression a more attractive alternative to GPU programmers than existing technologies like Unified Memory oversubscription.

## 9. REFERENCES

- [1] L. Gu, J. Siegel, and X. Li, “Using GPUs to Compute Large Out-of-card FFTs,” in *Proceedings of the International Conference on Supercomputing*, ser. ICS ’11, 2011.
- [2] F. Song, S. Tomov, and J. Dongarra, “Enabling and scaling matrix computations on heterogeneous multi-core and multi-gpu systems,” in *Proceedings of the 26th ACM International Conference on Supercomputing*, ser. ICS ’12, 2012.
- [3] C. Peng, T. Xiao, Z. Li, Y. Jiang, X. Zhang, K. Jia, G. Yu, and J. Sun, “Megdet: A large mini-batch object detector,” *CoRR*, vol. abs/1711.07240, 2017.
- [4] X. Chen, D. Z. Chen, and X. S. Hu, “moDNN: Memory optimal DNN training on GPUs,” in *Proceedings of the Conference on Design, Automation, and Test in Europe (DATE)*, Mar. 2018, pp. 13–18.
- [5] M. Wang, C.-c. Huang, and J. Li, “Supporting Very Large Models using Automatic Dataflow Graph Partitioning,” *arXiv:1807.08887 [cs]*, Jul. 2018.
- [6] T. Akiba, T. Kerola, Y. Niitani, T. Ogawa, S. Sano, and S. Suzuki, “PFDet: 2nd Place Solution to Open Images Challenge 2018 Object Detection Track,” *arXiv:1809.00778 [cs]*, Sep. 2018.
- [7] M. Rhu, N. Gimelshein, J. Clemons, A. Zulfiqar, and S. W. Keckler, “vDNN: Virtualized Deep Neural Networks for Scalable, Memory-efficient Neural Network Design,” in *Proceedings of the International Symposium on Microarchitecture (MICRO)*, 2016, pp. 18:1–18:13.
- [8] M. Rhu, M. O’Connor, N. Chatterjee, J. Pool, Y. Kwon, and S. W. Keckler, “Compressing DMA Engine: Leveraging Activation Sparsity for Training Deep Neural Networks,” in *Proceedings of the International Symposium on High Performance Computer Architecture (HPCA)*, Feb. 2018, pp. 78–91.
- [9] M. Harris. (2016) Unified memory for CUDA beginners. NVIDIA Blog. [Online; accessed 18-Jan-2018].
- [10] T. Zheng, D. Nellans, A. Zulfiqar, M. Stephenson, and S. W. Keckler, “Towards high performance paged memory for gpus,” in *2016 IEEE International Symposium on High Performance Computer Architecture (HPCA)*. IEEE, 2016.
- [11] Ammar Ahmad Awan, Ching-Hsiang Chu, Hari Subramoni, Xiaoyi Lu, and Dhahaleswar K. Panda, “Can Unified-Memory support on Pascal and Volta GPUs enable Out-of-Core DNN Training?”
- [12] R. B. Tremaine, P. A. Franaszek, J. T. Robinson, C. O. Schulz, T. B. Smith, M. Wazlawski, and P. M. Bland, “IBM Memory Expansion Technology (MXT),” in *IBM Journal of Research and Development*, vol. 45, no. 2, 2001.
- [13] M. Ekman and P. Stenstrom, “A Robust Main-Memory Compression Scheme,” in *Proceedings of the 32nd Annual International Symposium on Computer Architecture*, 2005.
- [14] G. Pekhimenko, V. Seshadri, Y. Kim, H. Xin, O. Mutlu, P. Gibbons, M. Kozuch, and T. Mowry, “Linearly compressed pages: a low-complexity, low-latency main memory compression framework,” in *Proceedings of the 46th Annual IEEE/ACM International Symposium on Microarchitecture*, 2013.
- [15] J. Zhao, S. Li, J. Chang, J. L. Byrne, L. L. Ramirez, K. Lim, Y. Xie, and P. Faraboschi, “Buri: Scaling Big-Memory Computing with Hardware-Based Memory Expansion,” *ACM Trans. Archit. Code Optim.*, vol. 12, no. 3, 2015.
- [16] E. Choukse, M. Erez, and A. R. Alameldeen, “Compresso: Pragmatic Main Memory Compression,” in *Proceedings of the International Symposium on Microarchitecture (MICRO)*, 2018.
- [17] J. Nystad, A. Lassen, A. Pomianowski, S. Ellis, and T. Olson, “Adaptive scalable texture compression,” in *Proceedings of the Fourth ACM SIGGRAPH / Eurographics Conference on High-Performance Graphics*, ser. EGHH-HPG’12, 2012.
- [18] A. Jain, A. Phanishayee, J. Mars, L. Tang, and G. Pekhimenko, “Gist: Efficient Data Encoding for Deep Neural Network Training,” in *Proceedings of the International Symposium on Computer Architecture (ISCA)*, Jun. 2018, pp. 776–789.
- [19] NVIDIA. NVIDIA DGX-2: The world’s most powerful AI system for the most complex AI challenges. <https://www.nvidia.com/en-us/data-center/dgx-2/>.
- [20] N. Sakharnykh. (2016, December) Beyond gpu memory limits with unified memory on pascal. [Online]. Available: <https://devblogs.nvidia.com/beyond-gpu-memory-limits-unified-memory-pascal/>
- [21] —. (2018, March) Everything you need to know about unified memory. <http://on-demand.gputechconf.com/gtc/2018/presentation/s8430-everything-you-need-to-know-about-unified-memory.pdf>. GPU Technology Conference (GTC).
- [22] —. (2017) Unified memory on pascal and volta. GPU Technology Conference (GTC). [Online]. Available: <http://on-demand.gputechconf.com/gtc/2017/presentation/s7285-nikolay-sakharnykh-unified-memory-on-pascal-and-volta.pdf>
- [23] Tiffany Trader. (2017) TSUBAME3.0 points to future HPE Pascal-NVLink-OPA server. <https://www.hpcwire.com/2017/02/17/tsubame3-0-points-future-hpe-pascal-nvlink-opa-server/>. HPC Wire.
- [24] O. Consortium. OpenCAPI 3.0 Data Link Specification. [Online]. Available: <https://opencapi.org/wp-content/uploads/2016/09/OC-DL-Specification.10.14.16.pdf>
- [25] A. Caldeira. (2018, March) Ibm power system ac922 introduction and technical overview. [Online]. Available: <https://www.redbooks.ibm.com/redpapers/pdfs/redp5472.pdf>
- [26] P. Markthub, M. E. Belviranli, and S. S. Lee, J. S. Vetter, “DRAGON: Breaking GPU Memory Capacity Limits with Direct NVM Access,” in *Proceedings of the International Conference on High Performance Computing, Networking, Storage and Analysis (SC)*, 2018.
- [27] K. Lim, J. Chang, T. Mudge, P. Ranganathan, S. K. Reinhardt, and T. F. Wenisch, “Disaggregated memory for expansion and sharing in blade servers,” in *Proceedings of the International Symposium on Computer Architecture (ISCA)*, 2009.
- [28] “Apple Releases Developer Preview of OS X Mavericks With More Than 200 New Features.” 2013. [Online]. Available: <https://www.apple.com/pr/library/2013/06/10Apple-Releases-Developer-Preview-of-OS-X-Mavericks-With-More-Than-200-New-Features.html>
- [29] “zram: Compressed RAM based block devices,” 2012. [Online]. Available: <https://www.kernel.org/doc/Documentation/blockdev/zram.txt>
- [30] G. Pekhimenko, V. Seshadri, O. Mutlu, P. Gibbons, M. Kozuch, and T. Mowry, “Base-Delta-Immediate Compression: Practical Data Compression for On-Chip Caches,” in *Proceedings of the International Conference on Parallel Architectures and Compilation Techniques (PACT)*, 2012.
- [31] A. R. Alameldeen and D. A. Wood, “Frequent Pattern Compression: A significance-based compression scheme for L2 caches,” Technical Report 1500, Computer Sciences Department, University of Wisconsin-Madison, Tech. Rep., 2004.
- [32] J. Yang, Y. Zhang, and R. Gupta, “Frequent value compression in data caches,” in *Proceedings of the 33rd Annual IEEE/ACM International Symposium on Microarchitecture*, 2000.
- [33] X. Chen, L. Yang, R. Dick, L. Shang, and H. Lekatsas, “C-PACK: A High-Performance Microprocessor Cache Compression Algorithm,” in *IEEE Educational Activities Department vol. 18*, 2010.
- [34] J. Kim, M. Sullivan, E. Choukse, and M. Erez, “Bit-Plane Compression: Transforming Data for Better Compression in Many-Core Architectures,” in *Proceedings of the 43rd Annual International Symposium on Computer Architecture*, 2016.
- [35] Z. Jia, M. Maggioni, B. Staiger, and D. P. Scarpazza, “Dissecting the NVIDIA volta GPU architecture via microbenchmarking,” *CoRR*, 2018. [Online]. Available: <http://arxiv.org/abs/1804.06826>
- [36] L. Liu, L. L. Deng, X. Hu, M. Zhu, G. Li, Y. Ding, and Y. Xie, “Dynamic sparse graph for efficient deep learning,” *CoRR*, vol. abs/1810.00859, 2018.
- [37] A. Gruslys, R. Munos, I. Danihelka, M. Lanctot, and A. Graves, “Memory-efficient backpropagation through time,” in *NIPS*, 2016.
- [38] M. Rhu, N. Gimelshein, J. Clemons, A. Zulfiqar, and S. W. Keckler, “vdnn: Virtualized deep neural networks for scalable, memory-efficient neural network design,” *2016 49th Annual IEEE/ACM International Symposium on Microarchitecture (MICRO)*, pp. 1–13, 2016.
- [39] C. D. Sa, M. Leszczynski, J. Zhang, A. Marzoczy, C. R. Aberger, K. Olukotun, and C. Ré, “High-accuracy low-precision training,” *CoRR*, vol. abs/1803.03383, 2018.
- [40] Y. Ito, R. Matsumiya, and T. Endo, “ooc\_cudnn: Accommodating convolutional neural networks over GPU memory capacity,” in *2017 IEEE International Conference on Big Data (Big Data)*, Dec. 2017, pp. 183–192.
- [41] NVIDIA. NVIDIA Turing GPU Architecture. [Online]. Available: <https://www.nvidia.com/content/dam/en-zz/Solutions/design-visualization/technologies/turing-architecture/NVIDIA-Turing-Architecture-Whitepaper.pdf>
- [42] G. Pekhimenko, E. Bolotin, N. Vijaykumar, O. Mutlu, T. C. Mowry, and S. W. Keckler, “A case for toggle-aware compression for gpu systems,” *2016 IEEE International Symposium on High Performance Computer Architecture (HPCA)*, 2016.

[43] Y. Jia, E. Shelhamer, J. Donahue, S. Karayev, J. Long, R. Girshick, S. Guadarrama, and T. Darrell, “Caffe: Convolutional architecture for fast feature embedding,” in *Proceedings of the 22Nd ACM International Conference on Multimedia*, ser. MM ’14, 2014.

[44] G. Juckeland, W. C. Brantley, S. Chandrasekaran, B. M. Chapman, S. Che, M. E. Colgrove, H. Feng, A. Grund, R. Henschel, W. mei W. Hwu, H. Li, M. S. MÄijller, W. E. Nagel, M. Perminov, P. Shelepuhin, K. Skadron, J. A. Stratton, A. Titov, K. Wang, G. M. van Waveren, B. Whitney, S. Wienke, R. Xu, and K. Kumaran, “Spec accel: A standard application suite for measuring hardware accelerator performance.” 2014.

[45] A. Krizhevsky, I. Sutskever, and G. E. Hinton, “Imagenet classification with deep convolutional neural networks,” in *Proceedings of the 25th International Conference on Neural Information Processing Systems - Volume 1*, ser. NIPS’12, 2012.

[46] C. Szegedy, V. Vanhoucke, S. Ioffe, J. Shlens, and Z. Wojna, “Rethinking the inception architecture for computer vision,” *2016 IEEE Conference on Computer Vision and Pattern Recognition (CVPR)*, 2016.

[47] F. N. Iandola, M. W. Moskewicz, K. Ashraf, S. Han, W. J. Dally, and K. Keutzer, “SqueezeNet: Alexnet-level accuracy with 50x fewer parameters and <1mb model size,” *CoRR*, vol. abs/1602.07360, 2016.

[48] K. Simonyan and A. Zisserman, “Very deep convolutional networks for large-scale image recognition,” *CoRR*, vol. abs/1409.1556, 2014.

[49] K. He, X. Zhang, S. Ren, and J. Sun, “Deep residual learning for image recognition,” *2016 IEEE Conference on Computer Vision and Pattern Recognition (CVPR)*, 2016.

[50] J. Deng, W. Dong, R. Socher, L.-J. Li, K. Li, and L. Fei-Fei, “ImageNet: A Large-Scale Hierarchical Image Database,” in *CVPR09*, 2009.

[51] R. Józefowicz, O. Vinyals, M. Schuster, N. Shazeer, and Y. Wu, “Exploring the limits of language modeling,” *CoRR*, vol. abs/1602.02410, 2016.

[52] A. Arunkumar, E. Bolotin, B. Cho, U. Milic, E. Ebrahimi, O. Villa, A. Jaleel, C.-J. Wu, and D. Nellans, “Mcm-gpu: Multi-chip-module gpus for continued performance scalability,” in *Proceedings of the 44th Annual International Symposium on Computer Architecture*, ser. ISCA ’17, 2017.

[53] U. Milic, O. Villa, E. Bolotin, A. Arunkumar, E. Ebrahimi, A. Jaleel, A. Ramirez, and D. Nellans, “Beyond the socket: NUMA-aware GPUs,” in *Proceedings of the 50th Annual IEEE/ACM International Symposium on Microarchitecture*. ACM, 2017, pp. 123–135.

[54] V. Young, A. Jaleel, E. Bolotin, E. Ebrahimi, D. Nellans, and O. Villa, “Combining HW/SW mechanisms to improve NUMA performance of Multi-GPU systems,” in *Proceedings of the 51th Annual IEEE/ACM International Symposium on Microarchitecture*. ACM, 2018.

[55] NVIDIA. NVIDIA Pascal GPU Architecture. [Online]. Available: <https://www.nvidia.com/object/pascal-architecture-whitepaper.html>

[56] ———, NVIDIA Volta GPU Architecture. [Online]. Available: <https://images.nvidia.com/content/volta-architecture/pdf/volta-architecture-whitepaper.pdf>

[57] H. Qi, E. R. Sparks, and A. S. Talwalkar, “Paleo: a performance model for deep neural networks,” 2017.

[58] A. Krizhevsky, V. Nair, and G. Hinton, “Cifar-100 (canadian institute for advanced research).” [Online]. Available: <http://www.cs.toronto.edu/~kriz/cifar.html>

[59] P. Goyal, P. Dollár, R. B. Girshick, P. Noordhuis, L. Wesolowski, A. Kyrola, A. Tulloch, Y. Jia, and K. He, “Accurate, large minibatch sgd: Training imagenet in 1 hour,” *CoRR*, 2017.

[60] C. J. Shallue, J. Lee, J. Antognini, J. Sohl-Dickstein, R. Frostig, and G. E. Dahl, “Measuring the effects of data parallelism on neural network training,” *arXiv preprint arXiv:1811.03600*, 2018.